Demonstration of efficient beam-wave interaction for a MW-level 48 GHz gyroklystron amplifier

L. J. R. Nix[1,2], L. Zhang[1,2], W. He[3], C. R. Donaldson[1], K. Ronald[1,2], A. W. Cross[1,2], and C. G. Whyte[1]

[1] *Department of Physics, SUPA, University of Strathclyde, Glasgow, G4 0NG, Scotland, UK*

[2] *The Cockcroft Institute, Sci-tech Daresbury, Warrington, WA4 4AD, UK*

[3] *College of Electronic Science and Technology, Shenzhen University, Shenzhen, 518060, China*

The development of high-frequency RF linear accelerators (linacs) requires consideration of several technological challenges, such as electron bunch linearization. Presented in this paper is the design of the interaction circuit for a 48 GHz MW-level three-cavity gyroklystron amplifier, appropriate for application as a millimeter wave power source in a 4th harmonic linearizing system for an X-band linac. The output cavity is operated at the cylindrical $TE_{0,2,1}$ mode, while the input and buncher cavities are operated at the $TE_{0,1,1}$ mode. The interaction circuit has been designed using a combination of analytical calculations and particle-in-cell (PIC) simulations. The optimized gyroklystron is shown, through simulation, to deliver an output power of up to 2.3 MW with gain of 36 dB and efficiency of 44% at 48 GHz, when driven by a 140 kV, 37 A electron beam.

Keywords: gyroklystron, millimeter-wave high-power amplifier, particle-in-cell simulation, fast-wave vacuum electronic device.

Electronic mail: laurence.nix@strath.ac.uk

I. INTRODUCTION

A gyroklystron is a vacuum electronic device based on the cyclotron resonance maser (CRM) mechanism[1]. Gyroklystrons are generally capable of high power output at narrow bandwidth, as compared with gyrotron traveling wave amplifiers (gyro-TWAs) which are moderate power broadband amplifiers[2].

Gyroklystrons were first developed in 1967 at the Institute of Applied Physics (IAP) in Russia[3, 4]. Since then, they have attracted significant interest, especially in the field of radar systems. Notably, high-power gyroklystron-based radar systems have been developed both in Russia (RUZA, 35 GHz)[5] and the USA (WARLOC, 94 GHz)[6]. To reduce magnetic field strength requirements, some gyroklystron designs have been studied using second harmonic operation[7-9]. Most radar gyroklystrons have been developed at Ka-band (~36 GHz) and W-band (~94 GHz) frequencies, though D-band (~140 GHz) frequencies have also been considered[10]. The efficiency achievable by the gyroklystron has improved greatly since its conception with an overall efficiency close to 40%[11-13].

Gyroklystrons have also attracted interest in the field of accelerator physics. When designing an RF accelerator, a higher drive frequency generally allows for a higher operating gradient. For linacs with a few GeV electron beams, this will significantly reduce the size of the footprint and the construction costs of the accelerator. However, achieving the required power at very high frequencies is a major challenge when using linear beam O-type klystrons. It is an increasing trend to employ acceleration structures operating at X-band instead of the C- and S-bands in linacs. The X-band acceleration structures can be driven by O-type klystrons which are able to deliver 75 MW of output power[14]. However, the output power capability of the klystron drops dramatically with increasing operating frequency due to its small dimensions and the maximum beam current and voltage it can handle. At higher frequency, significant work has been published by several groups, most notably at SLAC and the University of Maryland, describing the study of gyroklystrons as candidates for future TeV linear colliders[15]. This work led to many advancements in the technical and theoretical understanding of gyroklystrons as illustrated, for example, by several high-power coaxial designs at different frequencies from ~8 GHz to ~22 GHz, each capable of delivering tens of MW of output power[16-19]. To achieve high-power handling capacity without use of coaxial designs, the IAP has carried out studies of high-order mode gyroklystrons, such as a 35.4 GHz gyroklystron predicted to be capable of delivering 15 MW of output power using $TE_{7,1,1}$ and $TE_{7,3,1}$ modes[20]. A $TE_{5,2,1}$ to $TE_{5,3,1}$ mode sequence at 30 GHz was also studied, again predicting 15 MW of output power[13].

An advanced X-ray free-electron laser (XFEL) is being developed by the CompactLight collaboration across Europe and Asia[21]. The acceleration structure was developed by the CLIC experimental team at CERN (Geneva, Switzerland)[22] and operates at 12 GHz. The XFEL was proposed to operate with a high repetition rate of 100 Hz for hard X-rays and 1000 Hz for soft X-rays. For an X-band acceleration structure, during the acceleration process, unavoidable nonlinearities in an electron bunch's energy profile are introduced by the accelerating fields. Additional correction systems, called linearizers, are required to achieve performance targets. The most well-developed and reliable technique is harmonic linearization, wherein an additional cavity at a harmonic of the main drive frequency is added[23-27]. The conventional klystron is challenging to produce sufficient output power to drive the harmonic linearizers for an X-band structure. The gyroklystron is not subject to the same limitations and therefore becomes an attractive solution.

A third harmonic linearizer which would be driven by a 36 GHz gyroklystron has been designed for the 12 GHz acceleration structures of CompactLight. UESTC (Chengdu, China) and the University of Strathclyde (Glasgow, UK) have carried out studies into Ka-band MW gyroklystrons for accelerator applications such as this[12]. Although the 3rd harmonic option and its associated amplifier display good performance, there remains significant interest in the option of a linearizer operating at a higher harmonic, as it could theoretically achieve similar results with lower power demand and a shorter overall length of the linearizer. Therefore, a linearizer operating at the 4th harmonic (48 GHz) of the accelerating frequency has also been proposed.

The output power of the gyroklystron will be fed into a SLED-II type compressor and then to drive the linearizer[28]. The pulse length required from the gyroklystron is 2 μs with a minimum output power of 2 MW at 48 GHz. The compressor also requires the flipping of the phase of the input signal by 180° in a maximum of 5 ns and as quickly as possible, which means the gyroklystron also requires a bandwidth larger than 200 MHz to properly amplify the driving signal. In this paper, the beam-wave interaction circuit of a gyroklystron as a suitable amplifier at this frequency is presented.

II. PRINCIPLES OF THE GYROKLYSTRON

In a gyroklystron, a gyrating electron beam in a strong axial magnetic field interacts with the TE resonance modes of a series cavities. Fig. 1 shows a schematic of a gyroklystron with a three-cavity configuration. The seed microwave signal is coupled into the input cavity and will modulate the electron beam. The electron beam will gradually be bunched in the drift tube and the bunching is further enhanced by the intermediate cavity. At the output cavity, the electron beam will strongly couple with the cavity mode. If the electrons arrive with the correct phase to lose their kinetic energy, the cavity electromagnetic field will gain energy to result in amplified microwave radiation and then can be coupled out through a microwave window.

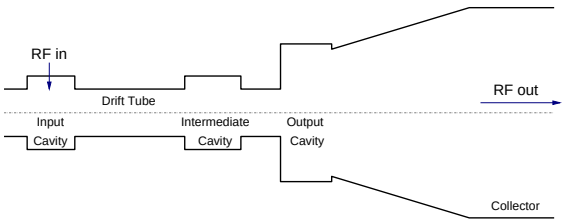

Fig. 1 Schematic diagram of a 3-cavity gyroklystron amplifier

It is of essential importance for the gyroklystron to have good phase-bunches to achieve high gain and high efficiency. Usually, having more intermediate cavities will help to reinforce the bunching process and achieve a higher gain. However, every additional cavity increases the complexity of the manufacturing process and assembly, as well as increasing the tolerance requirements. For the MW-level gyroklystron, low-quality factor cavities were used to avoid the oscillation, which results in large ohmic loss. The thermal issue would become increasingly challenging for a gyroklystron with more intermediate cavities because the energy stored in the later cavities is higher. For example, the energy stored in the third cavity of a four-cavity configuration can be more than three times compared with the 2nd cavity in a three-cavity configuration. Therefore, there is a trade-off between gain improvements, thermal issues, design complexity, and bunching quality that makes the decision of how many cavities to use non-trivial.

III. DESIGN OF THE GYROKLYSTRON

A good design of the gyroklystron requires the consideration of a lot of parameters, including those of the electron beam, the cavities, and the magnetic field. Since the gyroklystron was invented, a few models have been developed to describe the beam wave interaction process, including the small-signal linear theory with point-gap approximation[29], and the nonlinear theory[11, 30]. The linear theory provides a good starting point for the initial parameters such as the beam voltage, current, the transverse-to-axial velocity ratio α, and the magnetic field strength at the interaction region. The initial beam parameters chosen for the MW gyroklystron operating at 48 GHz are shown in Table 1.

Table 1. Initial parameters for the 48 GHz gyroklystron

Beam voltage (V_b)	140 kV
Beam current (I_b)	35 A
Transverse-to-axial velocity ratio (α)	1.35
Magnetic field strength (B_0)	2.02 T

The electron beam is generated from a magnetron injection gun (MIG)[31]. For a selected beam voltage, the resonance condition between the cyclotron frequency and cavity eigenmode can be satisfied by adjusting α and B_0 such that the dispersion relations meet tangentially at 48 GHz. A high velocity ratio can help improve interaction efficiency, however, the simulation on the MIG gun shows a higher velocity spread. The experience on the electron guns for gyro-devices indicates a larger spread in the experiments compared with the simulations, due to the intrinsic spread from the thermionic emission, especially operating at higher current density[32]. When α is larger than 1.5, back streaming electrons were also diagnosed in the measurement. Therefore, for the safe operation of the gyroklystron, as well as a balance of the interaction efficiency, the α value of 1.35 was chosen.

The operating modes selected for the gyroklystron are TE modes. Normally, low-order axially symmetric modes ($TE_{0,1,1}$ or $TE_{0,2,1}$) are used due to the electric field at the walls being low. For the MW-level gyroklystron, a relatively large beam current is used. If the cavity was larger in diameter with more modes available, there would be a greater risk of parasitic oscillations being excited due to the high current. However, a larger cavity than the $TE_{0,1,1}$ cavity is still desirable as the power-handling of a cavity is limited by its size. Therefore, the selected design consists of input and intermediate cavities operating at the $TE_{0,1,1}$ mode. The output cavity operates at the $TE_{0,2,1}$ mode as this allows it to be larger in diameter, thus enabling higher power handling capability while still maintaining strong stability and a reasonable coupling coefficient. The use of two compatible modes in this way is an effective technique, as the superior coupling coefficient and stability of the $TE_{0,1,1}$ mode are better for the input cavity compared with using the $TE_{0,2,1}$ for all cavities[33].

A three-cavity design was considered first. The initial linear theory analysis predicted that such a design was likely to meet requirements. A four-cavity option was also considered. Both of the design achieved similar efficiencies. The main benefit of additional cavities is to increase the gain, but the three-cavity device was able to achieve the required performance with less energy stored in the intermediate cavity, which is more important for stable operation. Therefore, assessing the relative challenges and merits in thermal stress, design complexity, and performance, the three-cavity option was chosen as a suitable balance between these aspects. It also has the additional benefit of being a suitable length to match the superconducting magnet currently available in the laboratory at Strathclyde.

After selecting the core beam parameters and general structure, the next step is to choose proper eigenfrequencies and Q factors for the cavities. Stagger-tuning is a technique in which cavity eigenfrequencies are slightly offset from the operating frequency, which is often utilized to increase the bandwidth of a gyroklystron to satisfy the requirement from the microwave compressor[29]. Appropriate stagger-tuned eigenfrequencies of the input and intermediate cavities can be estimated from the equations $f_0 + f_0/(3Q_0)$ and $f_0 - f_0/(3Q_0)$ respectively[34], where f_0 and Q_0 are the eigenfrequency and Q factor of the output cavity. Low-quality factor cavities are normally used in the high-power gyroklystron to avoid oscillation. The Q factors shown in Table 2 were chosen as the initial parameters for the three-cavity gyroklystron.

Table 2. Q factors of the cavities for the 48 GHz gyroklystron

Cavity	Q factor	Frequency (GHz)
Input	180	47.86
Intermediate	180	47.22
Output	100	47.70

The initial dimensions of the cavities were then estimated from the eigenfrequency and cavity eigenmode equations. If it is assumed that there is no leakage of microwaves into the drift tubes, the eigenfrequency f of the operating mode $TE_{m,p,n}$ can be written as Eq. 1

$$f = \frac{c}{\lambda_0} = \frac{c}{2\pi}\sqrt{\left(\frac{\nu_{mp}}{R}\right)^2 + \left(\frac{n\pi}{L}\right)^2} \quad (1)$$

where R and L are the radius and length of the cavity. At the same time, the guiding radius of the electron beam should be close to the position of the peak electric field strength of the operating mode to maximize the coupling coefficient, which is defined in Eq. 2 for a cavity mode $TE_{m,p,1}$ and a beam radius of r.

$$C_{mp}(r) = \frac{J_{m\pm1}^2(k_\perp r)}{\left(\nu_{mp}^2 - m^2\right)J_m^2(\nu_{mp})} \quad (2)$$

where J is the Bessel function of the first kind and ν_{mp} is the Bessel root corresponding to the mode in question. The ideal beam radius is slightly offset from the maximum coupling to account for the Larmor radius of electron orbit, as shown in Fig. 2. When the eigenfrequencies of the cavities are given, their radii and lengths can be calculated from Eq. 1 and 2. The selected beam radius was 1.77 mm.

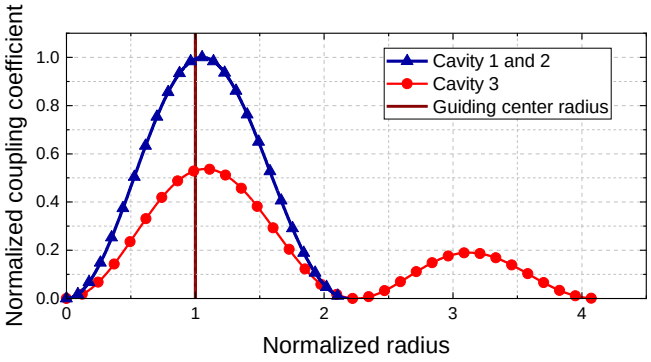

Fig. 2 Alignment between coupling coefficient and beam guide radius.

The output cavity is an open-ended structure with a discrete step in the structure. The eigenfrequency and Q factor were calculated by the mode-matching method[35]. By varying the taper angle and the depth of the iris, an output cavity structure meets the design requirements as detailed in Table 2. The output aperture radius had a large effect on Q factor and a small effect on eigenfrequency. The smooth output waveguide after the taper only had little effect on the eigenfrequency and Q factor. The field profile at the radius of the electron beam is shown in Fig. 3.

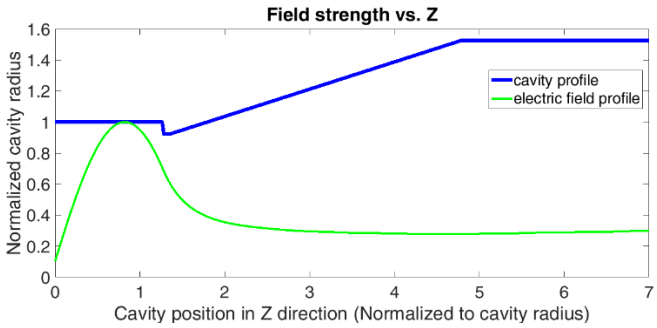

Fig. 3 geometry of the output cavity and the electric field profile of the operating mode $TE_{0,2,1}$.

The linear theory is not suitable for accurate design because the beam wave interaction is strongly nonlinear in high-power gyroklystrons. Also, the output cavity is open-ended and has significant differences to that of a closed cavity, which is not considered in the point-gap linear theory. The nonlinear theory, which can include the accurate field profiles of the cavities in the calculation and solve the beam-wave coupling equation (Eq. 3), is able to provide more accurate results for the gain and interaction efficiency[8].

$$\frac{dP}{dz} + i\frac{\gamma}{u_z}\left(\frac{\omega}{s} - \frac{\Omega_0}{\gamma}\right)P = -\frac{i\eta_0\gamma}{2u_z}C_{mn}k_{mn}J_{m-s}(k_{mn}R_e) \cdot \frac{F(z)}{(s-1)!}\left(\frac{k_{mn}P^*}{2\Omega_0}\right)^{s-1} i^{s-1} \quad (3)$$

$$\left(\frac{d^2}{dz^2} + \frac{\omega^2}{c^2} - k_{mn}^2\right)F(z) = -\mu_0\omega I_0 C_{mn}k_{mn}J_{m-s}(k_{mn}R_e) \cdot \frac{1}{2^s u_z}\frac{s}{(s-1)!}\left(\frac{-ik_{mn}}{\Omega_0}\right)^{s-1}\frac{1}{2\pi}\int_0^{2\pi} P^s d\Lambda_0 \quad (4)$$

where $P = iu_t \exp\{-i[\Lambda + (1 - m/s)\phi_e]\}$ describes the transverse component of the electron momentum, u_t and u_z are the transverse and axial components of the normalized momentum u, $\Lambda = (\omega/s - \Omega)\tau + \omega/st_0 - \phi$ is the slowly varying component of the phase, Λ_0 is the initial gyro-phase, I_0 is the beam current, s is the harmonic number, Ω is the cyclotron frequency for the electron, ϕ describes the angular modulation, ϕ_e is the polar angle of the guiding center, τ is the time since the particle entered the current stage, k_{mn} is the transverse wavenumber, and R_e is the guiding center radius. $F(z)$ is the electric field profile along the z axis.

The nonlinear theory provides a balance between accuracy and simulation time. It is able to provide useful information on the bunching process and the trends that occur when changing the parameters. The initial dimensions of cavities, as well as the length of the drift tubes from the linear theory, were then further optimized using the nonlinear theory calculations to achieve optimal efficiency. The maximum interaction efficiency was about 40%. Fig. 4 shows the interaction efficiencies at the intermediate and output cavity as the function of the cavity positions, where the position 0 denotes the starting point of the cavity.

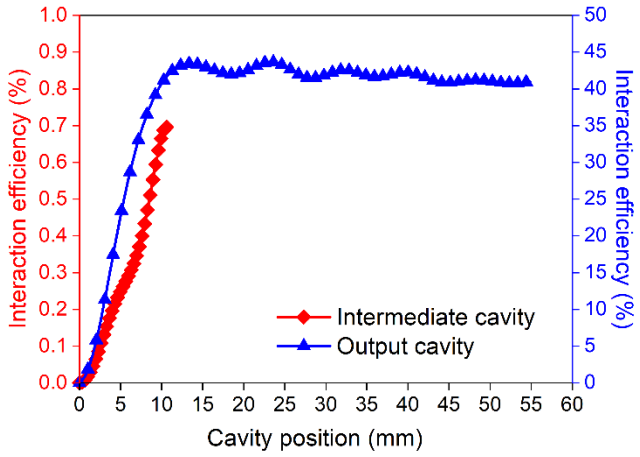

Fig. 4 interaction efficiency at the intermediate and output cavities

IV. PIC SIMULATION OF THE GYROKLYSTRON

The particle-in-cell code simulation method provides increased accuracy at the cost of much larger computation time. This makes it suited to final optimization and validation, sweeping across a range of parameters. Here, the finite-difference time-domain PIC code MAGIC[36] was used to validate the design from the nonlinear theory prediction and further improve the gyro-klystron performance.

In MAGIC simulations, the cavities were first simulated individually to ensure the correct eigenfrequencies and field patterns when the dielectric material was applied. Fig. 5 shows an example of the azimuthal electric field pattern of the intermediate cavity. The gyroklystron cavity dimensions as finalized after MAGIC analysis are shown in table 3.

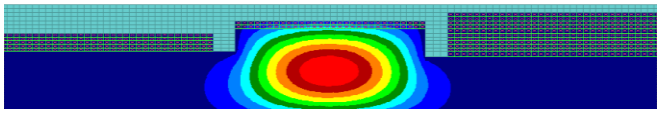

Fig. 5 Field pattern of the azimuthal E-field component of a $TE_{0,1,1}$ mode in the input cavity.

Table 3. Dimensions of the cavities and drift tubes.

Section	Radius (mm)	Length (mm)
Cavity 1	3.88	8.66
Drift tube 1	2.50	20.00
Cavity 2	3.88	10.20
Drift tube 2	2.50	7.20
Cavity 3	7.28	9.60

Dielectric linings are included in the cavities to introduce additional loss and reduce the Q factor. The dielectric material used is SiC due to its high loss tangent[37]. The thickness in the input and intermediate cavities are 0.7 mm and 0.3 mm, respectively.

The cavities were then assembled with the drift tubes to simulate the performance of the whole gyroklystron. The initial parameter set from the nonlinear theory achieved a steady output power of around 1.7 MW, with 34 dB gain. Further PIC simulations were performed to sweep across various input parameters, such as beam voltage, beam current, detuning parameter, and drive frequency. Figure 6 shows the start-oscillation current for modes in the output cavity using the linear gain theory. The start-oscillation current of the operating mode was 59 A. The output power can therefore be further increased using a higher beam current. With a slight increase in the beam current from 35 A to 37 A, the output power achieved was 2 MW. For this new current value, the performance characteristics were analyzed over a range of input power values as shown in Fig. 7.

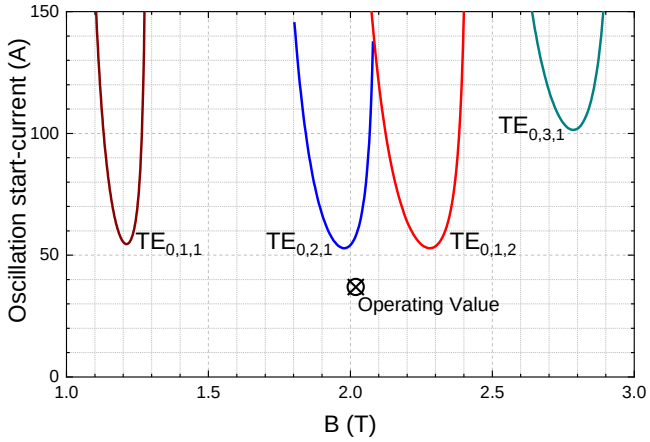

Fig. 6 Oscillation start-current for various modes in the output cavity

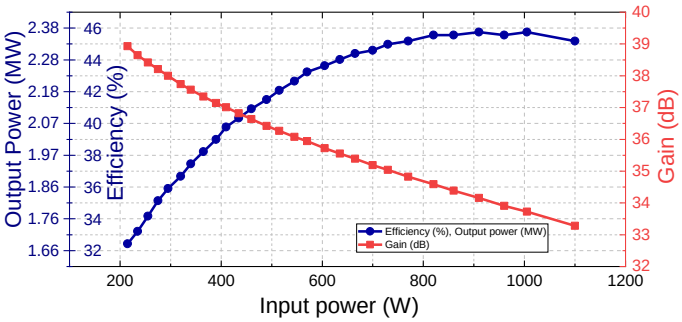

Fig. 7 Variation of the efficiency, gain and output power as the function of the input power.

Fig. 7 shows the variation of efficiency, gain, and output power as the function of input power. Increasing the drive power in the input cavity improves efficiency, but with diminishing returns in the output power. For example, at an input power of 295 W, the gyroklystron still operated in the linear gain region. The gain was as high as 38 dB, which enabled 1.9 MW of output power. Increasing the input power enables a higher output power, but the gain drops. For example, when doubling the input power to 605 W the output power increased to 2.3 MW; i.e. by a modest amount (~20%). At an input power of over 910 W, the output began to saturate, and the saturated gain was 34 dB. As the results already demonstrated output power above the 2 MW minimum target, further increase in input power was deemed unnecessary and 605 W was chosen as the input power value above which further investment in input power offers too little reward to be worthwhile. With the selected values of 605 W of drive power and a 140 kV, 37 A beam, the predicted

output power is 2.3 MW with 36 dB gain and 44% efficiency. The velocity spread of the electron beam was also introduced in the simulation to study its impact on the output power, as shown in Fig 8. The larger the velocity spread is, the larger the impact on output power becomes. The highest velocity spread for which the 2 MW requirement is met is slightly above 4%, by which point a 10% drop in output power was observed. Higher spread continued to reduce performance up to a value of 10%, above which oscillation at the output power was observed, and the gyroklystron ceases to maintain a stable operation.

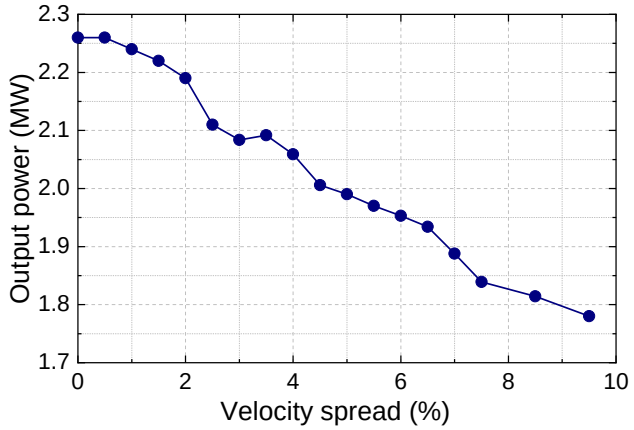

Fig. 8 Variation of output power with velocity spread.

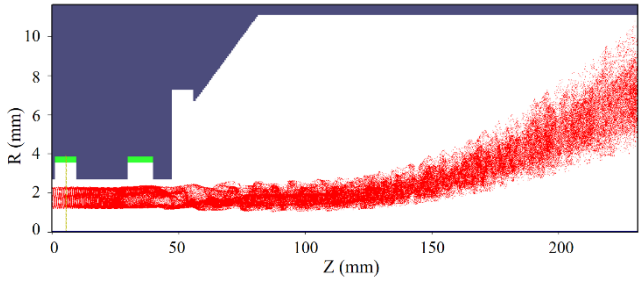

Fig. 9 Phase space plot of the electrons in the gyroklystron.

Fig. 9 shows the phase space plot of the electrons in the gyroklystron, demonstrating the interaction and subsequent deposition of the beam. The output power as a function of time is displayed in Fig. 10(a). After around 20 ns, the output power settles to 2.3 MW. The output power is reasonably steady, with fluctuations of less than 2%, which is mainly caused by the time-varying beam emission model used in the MAGIC simulations. The mode-purity of the outgoing radiation is also important to consider, as it can affect the performance of subsequent mode converters. The Fourier analysis of the output power is displayed in Fig. 10(b), which shows a clear peak at 48 GHz. A secondary peak is visible at 96 GHz, which is the second harmonic. The ratio of squared amplitudes for the fundamental to the second harmonic components is 21.

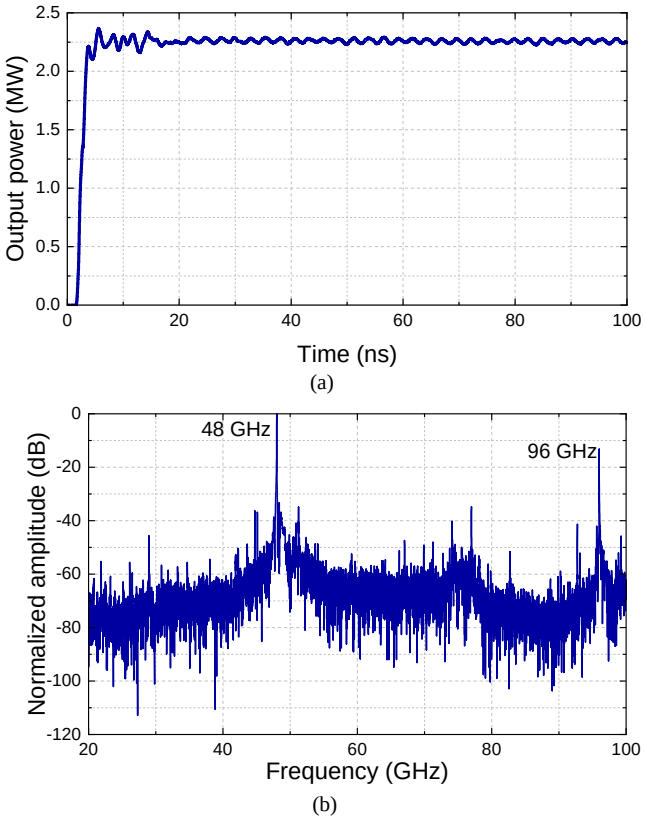

Fig. 10 Output power (a) and the spectrum of the output signal (b).

The bandwidth of the gyroklystron was also simulated and the results are shown in Fig. 11. The 3 dB bandwidth is about 400 MHz, which satisfies the minimum bandwidth requirement from the microwave compressor.

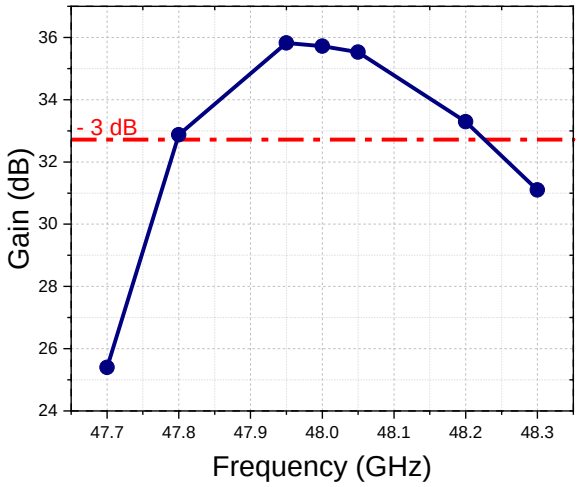

Fig. 11 Variation of gain with operating frequency.

Higher output power is possible with the use of a higher beam current. As displayed in Fig. 12, the simulations showed a linear increment of the output power when the electron beam increased up to 53 A, beyond which oscillation occurred. However, several limiting factors exist with regard to increasing the current. Higher beam current pushes the thermionic MIG gun to operate at higher current density,

which is already at its limit and will significantly reduce its lifetime. Also increasing the beam current will result in larger space-charge effect. It is challenging to maintain the velocity spread of the electron beam under the design criteria of 4% at a higher current. The 37 A beam current is still chosen as main operation parameter for a safe operation.

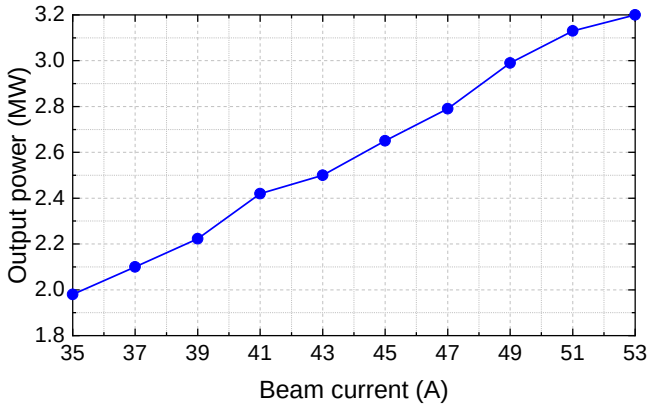

Fig. 12. Variation of output power with beam current

V. Conclusion

In this paper, the design of a three-cavity $TE_{0,1,1}$-$TE_{0,1,1}$-$TE_{0,2,1}$ 48 GHz gyroklystron amplifier has been presented. It was designed with consideration of the requirements of a harmonic linearizer operating at the 4th harmonic of the 12 GHz linac drive frequency used in CompactLight. The choice to use the 4th harmonic rather than the 3rd allows for a shorter linearizer and lower power demand. Vacuum electronic devices around 48 GHz have previously received little attention, so the new development of an appropriate amplifier was required. The gyroklystron designed here using a combination of linear calculations, nonlinear analysis, and PIC simulations represents a viable microwave source for application within the linearizer system. Following optimization using PIC simulations, an output power of 2.3 MW with a gain of 36 dB and an efficiency of 44% has been predicted when using a 140 kV, 37 A electron beam. The effect of the velocity spread was also studied. A 4% velocity spread will result in 10% drop in the output power, but still larger than 2 MW. The 3 dB-bandwidth is 400 MHz.

This work is supported by CompactLight, which has received funding from the European Union's Horizon 2020 research and innovation programme under grant agreement No. 777431. The authors would like to thank the Engineering and Physical Sciences Research Council (EPSRC), and the Cockcroft Institute, UK for supporting this work.

1. J. L. Hirshfield and J. M. Wachtel, Physical Review Letters **12** (19), 533-536 (1964).
2. L. R. Barnett, IEEE Transactions on Electron Devices **28** (7), 872-875 (1981).
3. I. I. Antakov, et. al. International Patent Number: 302050 (1967).
4. A. I. Gaponov, M. U. Petelin and V. K. Yulpatov, Izvestiya Vuz. Radiofizika **10** (9-10), 1414-1453 (1967).
5. A. A. Tolkachev, et. al. IEEE Aerospace and Electronic Systems Magazine **15** (7), 25-31 (2000).
6. G. J. Linde, M. T. Ngo, B. G. Danly, W. J. Cheung and V. Gregers-Hansen, IEEE Transactions on Aerospace and Electronic Systems **44** (3), 1102-1117 (2008).
7. E. V. Zasypkin, M. A. Moiseev, I. G. Gachev and I. I. Antakov, IEEE Transactions on Plasma Science **24** (3), 666-670 (1996).
8. Z.-H. Geng and P.-K. Liu, IEEE Transactions on Plasma Science **34** (3), 534-540 (2006).
9. S.-X. Xu, et. al. IEEE Transactions on Plasma Science **40** (8), 2099-2104 (2012).
10. M. V. Swati, M. S. Chauhan and P. K. Jain, IEEE Transactions on Plasma Science **44** (11), 2844-2851 (2016).
11. M. S. Chauhan, M. V. Swati and P. K. Jain, Physics of Plasmas **22**, 033111 (2015).
12. L. Wang, et.al. IET Microwaves, Antennas & Propagation (2018).
13. N. I. Zaitsev, et. al. Journal of Communications Technology and Electronics **59** (2), 164-168 (2014).
14. D. Sprehn, et. al. AIP Conference Proceedings **807** (1) (2006).
15. V. L. Granatstein and W. Lawson, IEEE Transactions on Plasma Science **24** (3), 648-665 (1996).
16. W. Lawson, et. al. Physical Review Letters **81** (14), 3030-3033 (1998).
17. W. Lawson, IEEE Transactions on Plasma Science **33** (2), 858-865 (2005).
18. P. Purohit and W. Lawson, AIP Advances **3** (8), 082134 (2013).
19. K. R. Chu, V. L. Granatstein, P. E. Latham, W. Lawson and C. D. Striffler, IEEE Transactions on Plasma Science **13** (6), 424-434 (1985).
20. N. I. Zaitsev, et. al. Radiophysics and Quantum Electronics **48** (10-11), 737-740 (2005).
21. A. Mak, P. Salén, V. Goryashko and J. Clarke, (CompactLight Design Reports, 2018).
22. M. Aicheler, et. al. (CLIC Design Reports, CERN, 2012).
23. T. I. Smith, Nuclear Instruments and Methods in Physics Research, A **250** (1), 64-70 (1986).
24. M. Dehler, et. al. Physical Review Special Topics. Accelerators and Beams **12** (6), 062001 (2009).
25. T. Schietinger, et. al. Physical Review Accelerators and Beams **19** (10), 100702 (2016).
26. G. D'Auria, et al. Proceedings of IPAC'10, 2173-2175 (2010).
27. G. D'auria, S. Di Mitri, G. Penco and C. Serpico, Proceedings of IPAC'12, 1721-1723 (2012).
28. P. B. Wilson, Z. D. Farkas and R. D. Ruth, Proceedings of the Linear Accelerator Conference, 204-206 (1990).
29. G. S. Nusinovich, B. G. Danly and B. Levush, Physics of Plasmas **4** (2), 469-478 (1997).
30. T. M. Tran, et. al. Physics of Fluids **29** (4), 1274-1281 (1986).

31. G. S. Kino and N. J. Taylor, IRE Transactions on Electron Devices **9** (1), 1-11 (1962).
32. S. E. Tsimring, Radiophysics and quantum electronics **15** (8), 952-961 (1972).
33. C.-H. Du and P.-K. Liu, *Millimeter-Wave Gyrotron Traveling-Wave Tube Amplifiers*, 2014 ed. (Springer, Berlin, Heidelberg, 2014).
34. J. P. Calame, et. al. Physics of Plasmas **6** (1), 285-297 (1999).
35. L. Zhang, W. He, C. R. Donaldson and A. W. Cross, Journal of Infrared, Millimeter and Terahertz Waves **37** (9), 846-856 (2016).
36. L. Ludeking, D. Smithe and G. Warren, Computer Physics Communications **87** (1-2), 54-86 (1995).
37. Y. Takeuchi, T. Abe, T. Kageyama and H. Sakai, Proceedings of the 2005 Particle Accelerator Conference **2005**, 1195-1197 (2005).